Temporal Fluctuations in a 100-A LaB_6 Hollow Cathode

IEPC-2013-385

Presented at the 33rd International Electric Propulsion Conference,
The George Washington University, Washington, D.C., USA
October 6–10, 2013

Benjamin A. Jorns* and Ioannis G. Mikellides† and Dan M. Goebel ‡
Jet Propulsion Laboratory, California Institute of Technology, Pasadena, CA 91109, USA

The temporal fluctuations in the near plume of a 100-A LaB_6 hollow cathode are experimentally investigated. A probe array is employed to measure the amplitude and dispersion of axial modes in the plume, and these properties are parametrically examined as a function of cathode operating investigations. The onset of ion acoustic turbulence (IAT) is observed at high current values, and the character of the turbulent spectrum is shown to agree with weak turbulent theory: the amplitude of the spectrum decreases with flow rate but increases with discharge current while the shape of the spectrum at high frequencies is characterized by Kadomtsev decay. Estimates of the anomalous collision frequency based on experimental measurements indicate that the IAT collision frequency can exceed the classical rate at high discharge current densities and that the magnitude of the anomalous collision frequency is sufficient to explain deviations of the experimentally-observed parameters from classical predictions. Additionally, the growth of the IAT is shown to be correlated with the appearance of a high energy ion tail.

I. Introduction

Despite the fact that the hollow cathode is a staple of many of the electric propulsion systems flown today, there are two major physical mechanisms governing the behavior of these flight-critical elements that remain unclear. The first is the presence of anomalous resistivity in the cathode plume.[1] Without a knowledge of this effect, simulations of hollow cathodes must be informed by experimental measurements. This dependence limits the ability of models to examine new design iterations and curtails their predictive capability for long life behavior. The second anomalous effect is the production of ions in the cathode plumes with energy significantly in excess of the discharge voltage. These high energy ions have been shown to be capable of completely eroding away the cathode keeper face[2,3]—a result which typically results in component failure.

To date, our lack of understanding of the cathode physical processes has not prevented the successful qualification of deep-space missions that rely on this technology;[4–7] however, in light of new NASA programs that are calling for higher power EP missions with extended lifetimes, it is becoming increasingly important to resolve the hollow cathode unknowns. For example, a recent proposal of the NASA In-Space Propulsion Project, Game Changing Development (GCD) Program requires 50-200 A cathodes with life capability that greatly exceeds 15,000 h. The only extended lifetime study of a high-current hollow cathode ever performed, however, fell far short of this goal with a maximum lifetime of only 8000 hours at 100 A.[8] In view of this failing, the need is apparent to design cathodes with improved capability, and a more complete understanding of the anomalous processes governing cathode behavior can help facilitate this effort.

While most investigations into the anomalous effects of hollow cathodes have focused on the problem of high energy ion formation,[9–17] the importance of anomalous collisions to cathode operation has only recently come to light. In particular, while attempting to simulate the NSTAR discharge cathode, Mikellides et al. found that it was necessary to invoke an anomalous collision term in order to match their modeling

*Associate Engineer, Electric Propulsion Group, benjamin.a.jorns@jpl.nasa.gov
†Principal Engineer, Electric Propulsion Group
‡Senior Research Scientist, Thermal and Propulsion Engineering Section

results to the experimentally-observed steady-state plasma parameters.[1,16] In an effort to provide a physical explanation as to why these anomalous collisions should exist, Mikellides et al. showed that the conditions in the hollow cathode plasma are suitable for the onset of ion acoustic turbulence (IAT)— a mode commonly found in current-carrying plasmas and often associated with significant anomalous collisonality.[18–20] The authors then argued that the collision frequency that arises from the IAT exhibits the correct dependence on plasma parameters—the so-called Sagdeev scaling[21]— to explain the anomalous resistivity that occurs in the hollow cathode plume.

In spite of this reasonable justification and the success the authors found in using the IAT collisionality to capture a number of experimentally-observed trends, Mikellides et al. noted that the incorporation of this effect into their models was based on conjecture: there was no experimental confirmation of the IAT. To be sure, acoustic modes have been proposed to explain some of the salient trends in the observed frequency spectra of probes inserted in the hollow cathode plume,[22,23] but the acoustic nature of these waves has never been directly measured. This lack of experimental confirmation brings a number of questions to mind about the role of the IAT in hollow cathode operation: Does the IAT even exist in the plasma plume? Does it result in anomalous collision frequency? If yes, does the collisionality correspond to the Sagdeev scaling employed in previous simulations? And is the magnitude of the collisionality sufficient to justify the use of anomalous resistivity in the models?

The goal of this paper is to examine these questions experimentally and analytically. In the first section, we briefly review the theory of current-driven turbulence in an unmagnetized plasma. In the second section, we describe the experimental setup we employed to probe for the presence of acoustic turbulence and its effects in the plume of a 100-A LaB_6 hollow cathode. In the third section, we present the results of the experimental investigation and interpret them in the context of both turbulent theory and simulations of the cathode that were performed for a companion paper.[24] We also briefly examine the correlation between IAT turbulence and the formation of a high-energy ion tail. In the fourth and final section, we discuss the implications of IAT for hollow cathode performance and future modeling efforts.

II. Ion Acoustic Turbulence Theory

The ion acoustic instability is an electrostatic mode that naturally arises in plasmas where there is a large disparity in ion and electron temperatures $T_e/T_i \gg 1$ and where there is a significant electron drift velocity V_e. As such, hollow cathode plumes with their strong electron current and low ion temperature are a prime environment for the onset of this wave. In this section, we review the dispersion relation for the acoustic mode, and we examine the impact the instability can have on steady-state plasma parameters.

A. Linear Dispersion Relation

Since the collisionless processes that lead to the growth of the ion acoustic mode are inherently kinetic, we examine its dispersion relation through this formalism. Implicit in the following derivation is that the plasma is uniform as compared to the wavelength $\lambda \ll L$ where L denotes the characteristic gradient length and that the wave vector k is in the same direction as the electron drift V_e. While this second assumption can be violated for large amplitude waves (c.f. Refs. 18 and 21) where loss processes lead to a saturation of modes in the parallel direction, we assume saturation is sufficiently weak at the onset of the instability that propagation is primarily in the direction of the electron drift. With this in mind, allowing for weak collisionality, the dispersion relation for acoustic modes is given by[25]

$$k^2 \varepsilon(\omega, k) = 0 = k^2 - \frac{1}{2} \sum_{s=e,i} \frac{1}{\lambda_{ds}^2} \frac{Z_0'(\zeta^s)}{1 - 2i(\nu_s/kv_s) Z_0(\zeta^s)}, \tag{1}$$

where ε denotes the dielectric tensor, $\lambda_{ds} = \frac{q^2 n_s}{\epsilon_0 T_s}$ is the Debye length of the s species, and $Z_0(\zeta^s)$ is the plasma dispersion function:

$$Z_0(\zeta^s) = i\sqrt{\pi} e^{-(\zeta^s)^2} \left[1 + \text{erf}(i\zeta^s)\right] \tag{2}$$

$$\zeta^s = \frac{\omega + i\nu_s - kV_s}{k} \left(\frac{m_s}{2T_s}\right)^{1/2}. \tag{3}$$

Here ω is the wave frequency, k is the component of the wave vector parallel to the electron drift velocity, V_s is the drifting speed of the s species in the parallel direction, v_s is the thermal speed, T_s is the temperature in units of energy, m_s is the species mass, $n_e = n_i = n_0$ is the background plasma density, and ν_s denotes the collision frequency.

We consider the following ordering that is characteristic of the ion acoustic mode as well as the cathode plasma $v_i \ll c_s \ll V_e \ll v_e$. In this limit, it is only necessary to consider the cases where $|\zeta^e| \ll 1$ and $|\zeta^i| \gg 1$. This allow us to simplify Eq. 1 considerably

$$k^2\varepsilon = 0 = k^2 - \omega_{pi}^2\left[-\frac{m_i}{T_e} + \frac{3T_i}{m_i}\frac{k^4}{(\omega')^4} + \frac{k^2}{(\omega')^2}\right] \tag{4}$$
$$- i\left[-\frac{\omega'/k - V_e'}{\lambda_{de}^2 v_e}\left(\left(\frac{\pi}{2}\right)^{1/2} + \left(\frac{\pi}{2} - 1\right)\frac{\nu_e}{kv_e}\right) - \omega_{pi}^2\left(\frac{\nu_i}{\omega'}\left(\frac{k}{\omega'}\right)^2 + \left(\frac{\pi}{2}\right)^{1/2}\left(\frac{m_i}{T_i}\right)^{3/2}\frac{\omega'}{k}e^{-m_i\left(\omega'/k\right)^2/(2T_i)}\right)\right],$$

where $\omega_{pi} = \sqrt{q^2 n_0/\varepsilon_0 m_i}$ and we have transformed to the ion rest frame, $\omega' = \omega - kV_i$; $V_e' = V_e - V_i$. The solution of this equation for the frequency as a function of the wavenumber yields the dispersion of the acoustic mode. Finding the exact solution is difficult, however, in light of the equation's nonlinearity. Instead, we approximate the frequency dependence (c.f. Ref. 26, Chapter 4) by separating the dielectric tensor into its real and imaginary components: $\varepsilon(\omega, k) = \varepsilon_r + i\varepsilon_i$. Then, letting k be real, allowing $\omega' = \omega_r + \omega_i i$, and assuming a small growth rate, $\omega_i \ll \omega$, we can Taylor expand the dielectric function with respect to ω_r. This yields two equations

$$0 = \varepsilon_r(\omega_r, k) \tag{5}$$
$$\omega_i = -\frac{\varepsilon_i(\omega_r, k)}{\partial\varepsilon_r(\omega_r)/\partial\omega}.$$

Applying the first of these approximations to Eq. 4, we find

$$(\omega_r')^2 = k^2 c_s^2\left(\frac{1}{(\lambda_{de}k)^2 + 1} + 3\frac{T_i}{T_e}\right), \tag{6}$$

where $c_s = \sqrt{T_e/m_i}$ is the ion sound speed. This is the kinetic dispersion for the real frequency of the ion acoustic mode. In the limit of cold ions $T_i \ll T_e$ and large wavelengths $k\lambda_{de} \ll 1$, we can see that this mode propagates with the ion sound speed $v_\phi = \omega/k = c_s$, whence it derives its name. Recalling that $\omega' = \omega - kV_i$, we can express the dispersion in the laboratory frame:

$$\omega \approx k\left[c_s + V_i\right], \tag{7}$$

where we have, for simplicity, made the substitution $\omega_r \to \omega$.

From Eq. 4 and the second line of Eq. 6, the imaginary part of the frequency is

$$\omega_i = \frac{1}{2}c_s k\left[\left(\frac{V_e' - c_s}{v_e}\right)\left[\left(\frac{\pi}{2}\right)^{1/2} + \left(\frac{\pi}{2} - 1\right)\frac{\nu_e}{kv_e}\right] - \left(\frac{\pi}{2}\right)^{1/2}\left(\frac{T_e}{T_e}\right)^{3/2} e^{-T_e/2T_i}\right] - \frac{1}{2}\nu_i, \tag{8}$$

where we have made the simplification $\omega'/k \approx c_s$ in order to arrive at this compact form. In this expression, the first term stems from electron Landau damping, the second is from electron collisional damping, the third term represents ion Landau damping, and the fourth term is from collisional damping due to ions. Following Ref. 25, we note that subject to the conditions for the development of the ion acoustic mode, we have $(\nu_e/kv_e) \approx (\nu_e/\omega)(m_e/m_i)^{1/2} \ll 1$. We therefore can neglect the second term in the growth rate as compared to the role of electron Landau damping. This yields the simplified form

$$\gamma = 2\omega_i = c_s k\left[\left(\frac{V_e' - c_s}{v_e}\right)\left[\left(\frac{\pi}{2}\right)^{1/2}\right] - \left(\frac{\pi}{2}\right)^{1/2}\left(\frac{T_e}{T_i}\right)^{3/2} e^{-T_e/2T_i}\right] - \nu_i, \tag{9}$$

where γ is called the growth rate of the instability. The reason for this nomenclature stems from the fact that when $\gamma > 0$, the instability grows.

The kinetic interpretation of the first term in Eq. 9 can be understood in the context of inverse Landau damping where the linear wave-particle interaction is localized to the particles with velocities close to the phase velocity of the propagating mode. The consequence of this particle interaction is an irreversible process leading to the redistribution of particle energy in the vicinity of the phase velocity—a flattening of the velocity distribution. If there are more particles with velocities slightly below the wave phase velocity, i.e. the particle velocity distribution has a negative slope, the net effect will be a redistribution of energy to higher values at the expense of wave energy. On the other hand, if there are more particles with a velocity slightly above the wave phase velocity (a positive slope in the particle velocity distribution), the wave will gain energy at the expense of the particle energy. For a Maxwellian distribution, it is necessary for the drift velocity to exceed the wave phase velocity in order for this second process to occur. This condition on drift velocity translates directly to $V_e' > c_s$ for the ion acoustic instability, and in the limit of a collisionless plasma with $T_e \gg T_i$, we can see from Eq. 9 that this criterion corresponds to the necessary and sufficient condition for the onset of the instability ($\gamma > 0$).[21,27]

The second term of Eq. 9 stems from ion Landau damping and represents a sink on wave energy. It is dominant when $T_e \approx T_i$, and it is for this reason that ion acoustic waves typically are only unstable in low temperature plasmas where thermal equilibrium has not been achieved between the two particle species. There is no mechanism for inverse ion Landau damping in the ion acoustic case since this mode necessarily propagates in the rest frame of the ions.

The third term in Eq. 9 includes the effects of ion-species collisions. For the weakly ionized regime of the cathode plume, we anticipate this term to be dominated by ion-neutral instances. In this case, ν_i represents the dissipation of the wave by collisions of the ions that carry the mode with background neutrals. Assuming $T_e \gg T_i$, which is valid for the cathode plasma, this term becomes the dominant sink over ion Landau damping. Eq. 9 then can be simplified to

$$\gamma = \omega' \left[\left(\frac{\pi}{2} \right)^{1/2} \left(\frac{V_e'}{v_e} \right) - \frac{\nu_i}{\omega'} \right], \tag{10}$$

which embodies the linear effects of the growth of the instability due to inverse electron Landau damping and its dissipation to collisions.

B. Turbulent Spectrum

While the linear theory from Eq. 10 indicates the criterion for when the ion acoustic instability can be driven unstable, it also suggests that for sufficiently large frequency, *any* ion acoustic wave that satisfies Eq. 7 can grow. This can give rise to a number of modes that propagate concurrently—the subsequent mixing of which leads to the formation of so-called ion acoustic turbulence (IAT). Ultimately, however, even though all of these modes can be excited, this amalgamation of propagating waves cannot grow indefinitely— some process must arise for the turbulent spectrum to saturate. Since linear theory does not provide a mechanism for this saturation, we are forced to include the dissipative effects of higher order, nonlinear terms. To this end, we consider the kinetic equation for the steady-state power spectrum of the IAT first put forth by Kadomtsev[28]and modified to include ion-neutral collisions:[29]

$$0 = \left(\frac{\pi}{2} \right)^{1/2} \frac{V_e'}{v_e} - \frac{\nu_i}{k c_s} + \alpha \frac{T_i}{T_e} k \lambda_{de}^3 \frac{\partial \left[k^3 I_k \right]}{\partial k}, \tag{11}$$

where $I(k) = q^2 [\phi(k)]^2 / (T_e)^2 / V_k$ is the normalized power spectrum, $\phi(k)$ is the potential amplitude of the mode with wavenumber k, V_k is a characteristic volume in wavenumber space, and $\alpha = 32\pi(2/15)$. The first two terms contain the linear growth and dissipation while the second term contains both the effects of wave-wave coupling to lower frequency modes and nonlinear ion Landau damping.

Allowing the cutoff wavenumber to be $k = 1/\lambda_{de}$, we can integrate Eq. 11 to find the steady-state spectrum:

$$I(k) = \alpha \left(\frac{T_e}{T_i} \right) \frac{1}{k^3} \left(\frac{V_e'}{v_e} \log \left[\frac{1}{\lambda_{de} k} \right] - \frac{\nu_i}{\omega_{pi}} \left(\frac{2}{\pi} \right)^{1/2} \left[\frac{1}{k \lambda_{de}} - 1 \right] \right). \tag{12}$$

We in turn can convert this result to frequency space through the relations $\omega' \approx k c_s$ and $I(k) V_k = I(\omega') V_{\omega'}$:

$$I(\omega') = \alpha' \left(\frac{T_e}{T_i} \right) \frac{1}{(\omega')^3} \left(\frac{V_e'}{v_e} \log \left[\frac{\omega_{pi}}{\omega'} \right] - \frac{\nu_i}{\omega_{pi}} \left(\frac{2}{\pi} \right)^{1/2} \left[\frac{\omega_{pi}}{\omega'} - 1 \right] \right), \tag{13}$$

where we have folded the characteristic volumes into α'. This expression represents the steady-state IAT spectrum that results when the dominant processes in the plasma are inverse electron Landau damping for the growth of the wave and collisional and nonlinear processes for its dissipation. In the limit $\omega' \gg \nu_i$, Eq. 13 simplifies to

$$I(\omega') \propto \frac{1}{(\omega')^3} \log\left[\frac{\omega_{pi}}{\omega'}\right], \tag{14}$$

which is the so-called Kadomtsev spectrum[28] in frequency space.

This result indicates that with increasing frequency the amplitude of the ion acoustic turbulence should decay cubically. On the hand, from Eq. 13 we can see that at the low frequency end of the spectrum, ion collisions become dominant and prevent the growth of the wave. The spectrum therefore disappears at both extremes of frequency range, and as such, we can infer the existence of optimum. From Eq. 13 in the limit $\omega \ll \omega_{pi}$, the value of this optimum is

$$\omega^* = 4\nu_i \left(\frac{2}{\pi}\frac{m_i}{m_e}\right)^{1/2} \frac{v_\phi}{V_e'} \left(3 \log\left[\frac{\omega_{pi}}{\omega'}\right]\right)^{-1}, \tag{15}$$

where $v_\phi = c_s + V_i$ is the laboratory phase velocity of the ion acoustic instability. We thus find that in the presence of weak collisionality, the frequency at the maximum of the turbulent spectrum depends linearly on the ion-neutral collision frequency and inversely on the electron drift. This result is physical intuitive. At a fixed phase velocity and collision frequency, we can see from Eq. 10 and Eq. 13 that inverse Landau damping increases with electron drift velocity. This suggests that the frequency where the damping effect of the ion neutral collisions ($\sim \nu_i/\omega'$) will become comparable to the inverse Landau damping is driven to lower values. Conversely, at fixed phase velocity and drift velocity, we can see that with increasing collision frequency, higher frequencies still will be collisionally damped. The location of the maximum therefore should increase with the ion collision frequency. Since $\nu_i \propto n_n$, this correspondence in turn suggests a scaling of the maximum frequency with neutral particle density.

C. Anomalous Collision Frequency

As we have seen from Eq. 10 and Eq. 12, the main driver for positive growth of the IAT is inverse electron Landau damping. This suggests that the energy for the ion acoustic instability comes at the expense of electron velocity. Effectively, the electrons are slowed down to add energy to the propagating waves. This energy transfer is irreversible and consequently can be modeled by an effective collision frequency. Under the assumption of the Kadomtsev-like decay in an IAT spectrum that we derived in the previous section, weak-turbulent theory yields an effective term for the collisional frequency:[21]

$$\nu_{AN} \approx \omega_{pe} \frac{W}{n_0 T_e}. \tag{16}$$

Here ω_{pe} denotes the electron plasma frequency and W is the total energy density in the IAT given by

$$W = \frac{\varepsilon_0}{2}\frac{1}{V_k} \int \omega' \left[k\phi(k)\right]^2 \frac{\partial \epsilon_r}{\partial \omega'} d\mathbf{k}, \tag{17}$$

where the integral is over all of $\mathbf{k}$ space. We thus find the intuitive result from Eq. 16 that the larger the instability, the more energy it must extract from the electrons in order to be maintained.

It is possible to relate Eq. 16 to experimentally-measurable quantities under the assumption that the wavevector is confined to a small cone centered around the direction of electron drift. Coupled with the relations $\omega' \approx kc_s$ and Eq. 4, this assumption allows us to proximate the volumetric integral by an integral in one dimension:

$$\nu_{AN} = \frac{\omega_{pe}}{2T_e^2}\frac{1}{L_k} \int_{k_{min}}^{1/\lambda_{de}} \left[q\phi(k)\right]^2 dk, \tag{18}$$

where L_k is a characteristic length in k space and we have implemented bounds on the integral based on the points where Eq. 12 changes sign. Finally, we can convert to a frequency integral to find

$$\nu_{AN} = \frac{\omega_{pe}}{2T_e^2}\frac{1}{L_\omega}\int_{\omega_{min}}^{\omega_{pi}}\left[q\phi\left(\omega\right)\right]^2 d\omega \tag{19}$$

$$= \frac{\omega_{pe}}{2T_e^2}\sum_{\omega_{min}}^{\omega_{pi}}\left[q\phi\left(\omega\right)\right]^2, \tag{20}$$

where L_ω is a characteristic length in frequency space and we have written in the second line the integral as a sum over components in the frequency spectrum. From this expression we can see that provided we can confirm that the IAT is present and damped in the Kadomtsev sense, it is only necessary to measure the plasma density, electron temperature, and potential amplitude spectrum of the turbulence in order to estimate the anomalous collision frequency.

While Eq. 20 is an expedient formula for the collisional term provided we can directly measure the spectrum amplitude, we note that it is also possible to express the anomalous collision frequency in terms of only macroscopic parameters. To see this, we re-examine the anomalous collision frequency by explicitly taking into consideration the form of the Kadomtsev spectrum (Eq. 12). When this is done for our spectrum, we find (c.f. Ref. 21 and 29)

$$\nu_{AN} \approx \alpha^*\omega_{pe}\frac{T_e}{T_i}\int_{x_{min}}^{1}\left(\frac{V_e'}{v_e}\log\left[\frac{1}{x}\right]-\frac{\nu_i}{\omega_{pi}}\left(\frac{2}{\pi}\right)^{1/2}\left[\frac{1}{x}-1\right]\right)dx, \tag{21}$$

where $x = k\lambda_{de}$ and α^* is a constant with value given approximately by 0.01.[30] Only retaining the dominant terms in this integral yields

$$\nu_{AN} \approx \alpha'\omega_{pe}\frac{T_e}{T_i}\frac{V_e'}{v_e}. \tag{22}$$

This is the Sagdeev form of the anomalous collision frequency due to IAT.[21] The advantage Eq. 22 is that it represents a strictly kinetic phenomenon in terms of macroscopic parameters (drift velocity, electron temperature, and ion temperature). If we can confirm that the IAT is present and damped in the Kadomtsev sense, then we only need to measure these flow properties in order to estimate the collision frequency. Eq. 22 also has the advantage that it can be implemented in fluid plasma codes even though these codes inherently cannot model the particle motion that gives rise to the anomalous effects. We noted in Sec. I the success of incorporating this Sagdeev term into 2-D fluid simulations of the NSTAR discharge cathode[1,16] as well as our 100-A cathode.[24]

In sum, both Eq. 20 and Eq. 22 provide a means to estimate the collision frequency that results from IAT. However, in order to justify the use of these expressions, it first is necessary to determine experimentally if the IAT exists and if follows a Kadomtsev-like decay. This means a direct measurement of the IAT in the cathode plume. In the following sections, we describe the experimental setup and diagnostic suite we adopted to achieve this end.

III. Experimental Setup

In this section, we describe the cathode we investigated as well as the diagnostics we employed to examine the development and impact of ion acoustic turbulence.

A. Cathode Assembly

The 100-A cathode assembly (Fig. 1) in our experiment was designed with the purpose of achieving high current output. As reported in detail in Ref. 31, it consists of a graphite tube that houses a LaB_6 insert. A tungsten endplate with an orifice that is 12% the diameter of the cathode tube caps the end. The cathode tube is wrapped with a tantalum coaxial heater that in turn is housed in a graphite keeper. The ratio of the keeper orifice to the keeper diameter is 15%.

The setup was installed in the JPL High Current Test Facility, a 2.8 m x 1.3 m cylindrical chamber with vacuum maintained by two cryopumps. The base pressure of this facility was $\sim 10^{-7}$ T, and at the max flow

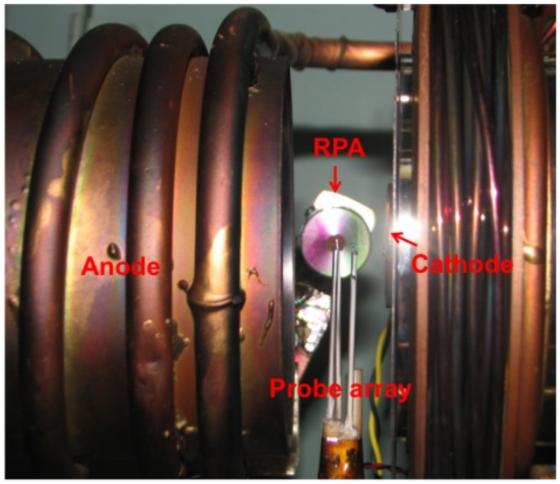

Figure 1. Photo of the 100-A hollow cathode employed in the experiment. The retarding potential analyzer and ion saturation probe array are also indicated.

condition we examined, 20 sccm xenon, the background pressure was maintained at 3.7×10^{-4} T. The anode consisted of a water-cooled, copper cylinder that was lined with tungsten and located ~ 3 cm downstream of the keeper face. The cathode assembly was surrounded by a solenoid capable of generating a magnetic field, though for the measurements reported here, there was no applied magnetic field.

B. Diagnostics

We performed three types of measurements during these trials in order to characterize the background plasma parameters, radial ion energy, and plasma fluctuations. We discuss in the following the diagnostics we employed to make these measurements and the analysis techniques we used.

1. Langmuir Probe

The background plasma density and temperature were measured with a single Langmuir probe located 0.75 cm downstream of the keeper face and placed on axis. The exposed element was 2 mm in length with a diameter of 0.51 mm. The reported electron temperature was inferred from an exponential fit to the probe IV trace (c.f. Ref. 32), while we employed the thin sheath approximation for cylindrical probes to estimate density, $n_i = i_{sat}/\left(0.61 q A_p \sqrt{T_e/m_i}\right)$ where A_p denotes the probe area. The measurements reported here were generated from an average of thirty-two probe traces.

2. Retarding Potential Analyzer

In order to characterize ion energy, we employed a four-grid, retarding potential analyzer (RPA) that was placed 0.75 downstream of the keeper face and 10 cm radially from the cathode axis. The first grid of the RPA was allowed to float while the second, electron repelling grid was biased negatively with respect to ground. The third and fourth grids were connected in parallel and provided the bias voltage necessary to resolve ion energies. The collector plate was grounded through a 1 MHz resistor, and we inferred the ion current from the drop across this resistor. We generated IV characteristics for this setup by sweeping the bias voltage from 0 to 100 V at 0.5 Hz and averaging over 16 traces.

The IV characteristics from the RPA can yield information on the distribution of ion-to-charge energies in the plasma. In particular, we have[33]

$$-\frac{dI}{dV} = \beta \sum_s q_s^2 \eta_s f_i^{(s)}\left(q_s V\right), \tag{23}$$

where β is a constant, q_s denotes the charge of the s ion species (e.g. singly, doubly, triply charged), η_s is the fraction of the ion density comprised of the s species, and $f_i^{(s)}$ is the energy distribution of the s ion species.

From this relation, it is evident that without a priori knowledge of the fraction of multiply charged states in the plasma, the interpretation of the IV characteristic is problematic. However, assuming the plasma is dominated by singly charge species, this expression is a proxy for the probability distribution of ion energy:

$$-\frac{dI}{dV} \approx \beta q^2 f_i \left(qV\right). \tag{24}$$

3. *Ion saturation probes*

To characterize the on-axis, current-driven fluctuations in the cathode plume, we employed the dual ion saturation probe setup shown in Fig. 1. It consisted of two exposed tungsten tips oriented along the axial direction. The length of each tip was 2 mm and each probe was biased to -30 V with a battery. The purpose of this diagnostic was to measure fluctuations ion saturation current i_{sat} since these in turn serve as a proxy for plasma potential. In particular, for electrostatic modes such as the ion acoustic wave, we have

$$\phi \approx \frac{T_e}{q}\frac{\tilde{n}}{n_0}, \tag{25}$$

where $\tilde{n}$ denotes the fluctuations in the plasma density. The ion saturation current, however, is a direct proxy for density $i_{sat} = \alpha n_i$ where α is a constant dependent on electron temperature and probe dimensions. Assuming electron temperature fluctuations are small compared to density perturbations then, we can see from Eq. 25 that

$$\phi \approx \frac{T_e}{q}\frac{\tilde{i}_{sat}}{\bar{i}_{sat}}, \tag{26}$$

where $\bar{i}_{sat}$ denotes the time averaged quantity. By measuring the fluctuations in ion saturation current, we thus are able to infer fluctuations in potential.

Armed with this relation, we can characterize the nature of waves in the plasma by correlating the signal between probe tips. The principle of this technique can be illustrated by representing the fluctuations in the plasma with an eikonal approximation:

$$\phi = \sum_k \phi\left(\omega\right) e^{i\left(k(\omega)x - \omega t\right)}, \tag{27}$$

where $k\left(\omega\right)$ is the wavenumber at frequency ω and $\phi\left(\omega\right)$ denotes the complex amplitude of the wave with frequency ω. The fluctuation in potential as measured at two different positions in x is thus measured as

$$\phi_1\left(t\right) = \sum_\omega \phi_1\left(\omega\right) e^{i\left(k(\omega)x_1 - \omega_k t\right)} \tag{28}$$

$$\phi_2\left(t\right) = \sum_\omega \phi_2\left(\omega\right) e^{i\left(k(\omega)x_2 - \omega_k t\right)}. \tag{29}$$

By taking the Fourier transform $\mathcal{F}$ with respect to time of these two signals, we can find the following relation:

$$k\left(\omega\right) = \frac{1}{\Delta x}\tan^{-1}\left[\frac{\mathrm{Im}\left(\mathcal{F}\left[\phi_2\left(t\right)\right]\mathcal{F}^*\left[\phi_1\left(t\right)\right]\right)}{\mathrm{Re}\left(\mathcal{F}\left[\phi_2\left(t\right)\right]\mathcal{F}^*\left[\phi_1\left(t\right)\right]\right)}\right], \tag{30}$$

where $\Delta x = x_2 - x_1$. This expression provides a means to measure the distribution of wavenumber $k\left(\omega\right)$ along the vector between the two probe tips (axial in our case) where the range of discernible wavenumber is dictated by the separation between probes, $|k| < \pi/\Delta x$.

The accuracy of this approach can be improved in a noisy environment by averaging over a number of time signals. However, if there are multiple modes present in the plasma, i.e. multiple wavenumbers for a fixed frequency, this technique can be errant. In order to resolve the distribution of k at a fixed ω, we employ the histogram technique first proposed by Beall.[34] In particular, we perform a number M of time samples and evaluate the wavenumber as a function of frequency for each run according to Eq. 30. We then bin the k values and weight them according to

$$S\left(\omega, k\right) = \frac{1}{M}\sum_{j=1}^{M} I_{0,\Delta k}\left[k - k^j\left(\omega\right)\right]\frac{1}{2}\left[P_1^{(j)}\left(\omega\right) + P_2^{(j)}\left(\omega\right)\right]. \tag{31}$$

Here j indicates the run number, $P_1^{(j)}, P_2^{(j)}$, are the power spectra of the two signals, and we have defined the function

$$I_{0,\Delta k}(x) = \begin{cases} 1 & 0 < \Delta k \\ 0 & |x| > \Delta k \end{cases}$$

where Δk is the width of of the bin. Eq. 31 provides a means for us to visualize the dominant frequencies and wavenumbers in $k-\omega$ space. In particular, the results for wave detection that we report in the following section were generated from Eq. 31 and are represented as intensity plots in $k-\omega$ with a wavenumber resolution of $\Delta k = 0.84$ m^{-1} (for 150 bins) and a frequency resolution of $\Delta f = 10$ kHz.

IV. Results

In the following section, we present the results of a parametric investigation of the oscillations in the plume of the 100-A LaB_6 cathode. All measurements were performed on axis at 0.75 cm from the keeper face. We examined operating conditions at four flow rates of xenon, 8 sccm, 10 sccm, 15 sccm, and 20 sccm over the discharge current range $I_D = 20$ A $- 130$ A.

A. Background measurements

We show measurements in Fig. 2 of the electron temperature and density as a function of the cathode operating condition. From the plot on the right hand side, we find the physically intuitive result that the density increases monotonically with discharge current at all flow conditions. Similarly, from the plot on the left, we immediately can see that the overall magnitude of electron temperature decreases with flow rate. This latter trend is consistent with previous experiment investigations[31] and suggests that collisional damping leads to an overall depression in electron temperature. The trends for temperature as a function of discharge

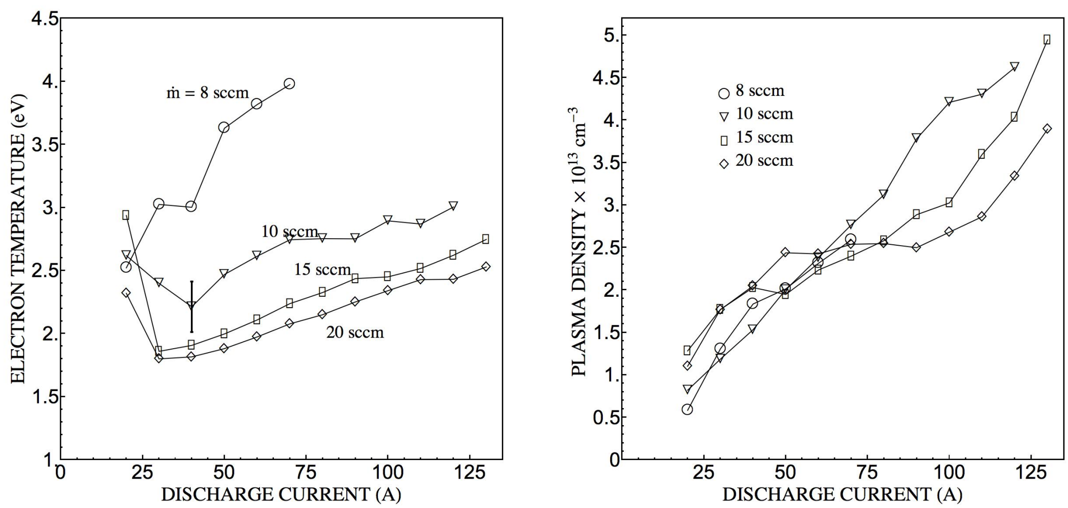

Figure 2. Electron temperature and density as functions of discharge current at four different flow rates. A representative error bar is shown for the temperature while the density is accurate to within 50%.

current are not as easily explained. In particular, at 8 sccm we can see the temperature strictly increases with discharge current, while at higher flow rates the electron temperature is non-monotonic—passing through a minimum value and then rising. This is in direct contrast to the results reported in Ref. 31 where it was found that *inside* the same cathode tube and at fixed flow rate, the electron temperature decreased monotonically with discharge current. This discrepancy between internal and external measurements may stem from the relationship between electron temperature and resistive heating in the plume. In particular, although the electron temperature falls inside the cathode with increasing discharge current due to internal processes, at sufficiently high discharge currents, local effects in the plume—such as the onset of the IAT—may give rise to enhanced collisionality. This in turn could lead to local heating and a subsequent increase in electron temperature. The initial decrease in temperature with current we observe in Fig. 2 thus could reflect the fact that at small discharge current, the resistive heating in the plume is sufficiently low that the plume temperature is a proxy for the internal cathode processes (decreasing temperature with current). It is only when the resistive effects in the plasma become sufficiently high that the external resistivity becomes dominant and the temperature in the plume deviates from the experimentally observed trends inside the cathode. This is a possibility we explore in the following sections.

B. Dispersion relation

In order to examine the nature of the fluctuations in the cathode plume, we employed the methods and techniques we outlined in Sec. III to generate the Beall intensity plots[34] shown in Fig. 3. These plots serve to illustrate the frequency and axial wavenumber character of the fluctuations in the cathode plume as a function of increasing discharge current at fixed flow rate (10 sccm). Most notably, we can see that while

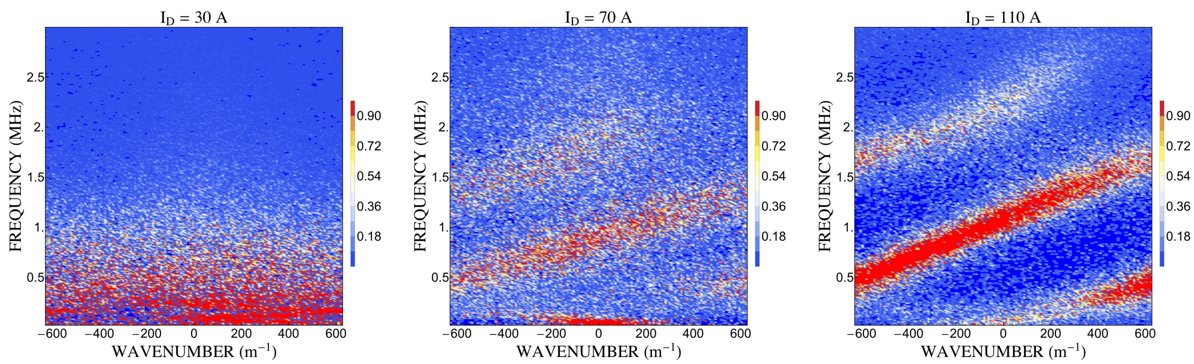

Figure 3. Beall plots with increasing current at the flow condition $\dot{m} = 10$ sccm. Each plot is normalized to its maximum and has a frequency resolution of 10 kHz.

at $I_D = 30$ A the intensity plot is dominated by low frequency (< 100 kHz) and dispersionless content, with increasing discharge current, a high frequency mode with a linear dispersion begins to emerge. This is clearly illustrated by the transition from $I_D = 70$ A to $I_D = 110$ A where in the former case the high frequency content is comparable in amplitude to the low frequency components and in the latter case the high frequency mode is dominant with a maximum near 800 kHz.

The strong linearity from both plots that exhibit the high frequency mode allows us to identify the effects of aliasing. Since the probe spacing is a finite width Δx, modes with wavelength λ shorter than the spacing between the probe tips appear as lower wavenumbers with $k = 2\pi\left(\lambda^{-1} - n/\Delta x\right)$ where $n = \lfloor \Delta x/\lambda \rfloor$. Given the periodicity of the dispersions in Fig. 3, however, we can adjust for the aliasing by translating the plot with respect to wavenumber. An example of this correction is shown in Fig. 4 and reflects the true dispersion of the mode.

The linear nature of the high frequency mode in the direction of electron drift strongly suggests that it is the ion acoustic instability ($\omega \propto k$). This conclusion is bolstered by measurements of the phase velocity exhibited by the mode, which we have made by fitting a line to the dispersion plot. An example of such a fit is illustrated by the dotted line in Fig. 4, and the results of these fits over the investigated parameter space is shown in Fig. 5. We note that the plotted points correspond to the conditions where we could observe the linear dispersion in the Beall plots, and the reason why the high flow rate case, $\dot{m} = 20$ sccm, is not shown is because we could not resolve the high frequency mode above the noise. For comparison, we also include in Fig. 5 a plot of the calculated sound speed $c_s = \sqrt{T_e/m_i}$ as a function of operating conditions. The correspondence between the measured phase velocity and the ion sound speed provides the strongest evidence yet that the observed linear mode is the ion acoustic instability. Admittedly, there is an offset in all cases of ~ 3 km/s such that the measured phase velocity does not correspond directly to the sound speed, but we note that this discrepancy can be explained by the fact that the phase velocity of the wave is the sum of the ion sound speed and the ion drift velocity (Eq. 7). This would indicate an axial ion drift of the ions of ~ 3 km/s, which is consistent with previous laser induced fluorescence measurements of ion velocities in

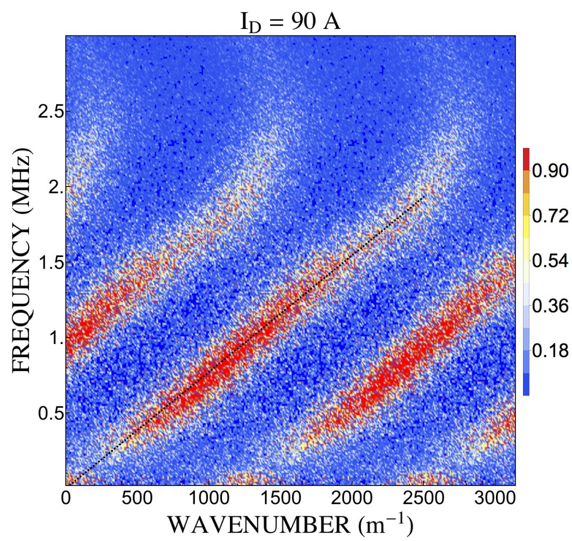

Figure 4. Beall intensity plot where aliasing is corrected for the case of $I_D = 90$ A and $\dot{m} = 10$ sccm. The dotted line is a best fit to the linear dispersion of the acoustic mode.

a hollow cathode[35] as well as simulations of our 100-A LaB_6 high current cathode.[24]

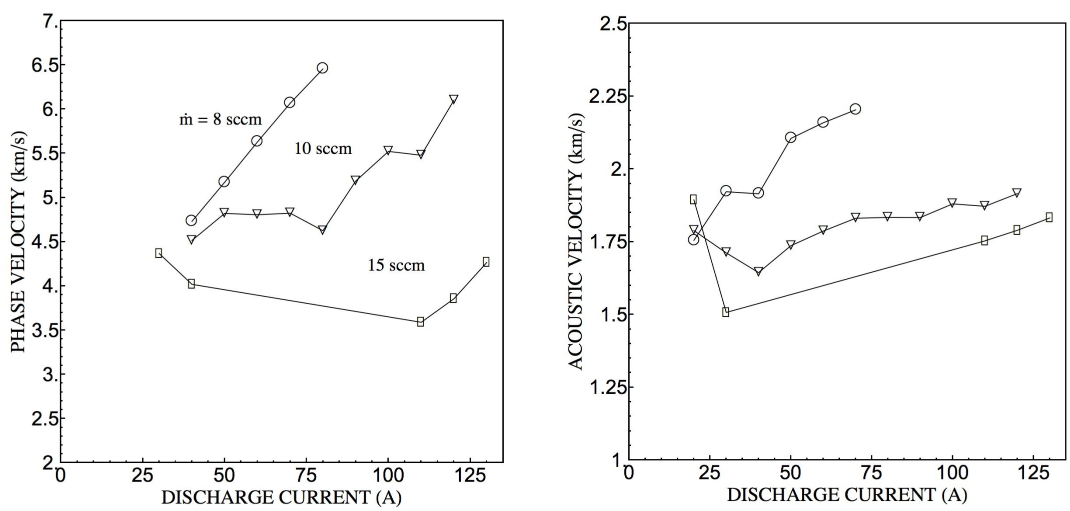

Figure 5. Left: Phase velocity of the acoustic mode as a function of discharge current at different mass flow rates. The IAT could not be resolved at $\dot{m} = 20$ sccm, and the absence of points in the $\dot{m} = 15$ sccm reflects our inability to detect the dispersion of the mode for these current values. Right: the calculated sound speed c_s at the same conditions.

In light of these results, we have for the first time experimental evidence that ion acoustic turbulence exists in the cathode plume. This corroborates the assumptions about the local plasma we made in Sec. II as well as the findings of previous modeling efforts that showed the conditions were right for this mode to exist.[1,16,24] Ultimately, however, proof that the mode exists is not sufficient to demonstrate that it plays an important role in the plasma processes of the cathode plume. We still need to determine the effective collision frequency that results from the IAT. While we already have arrived at an expression for this anomalous collision frequency in Sec. II, before we can apply it to our results, it is necessary to confirm that the IAT exhibits the type of spectrum we assumed in the theory. This is not an unreasonable expectation since we note that the IAT is generally dominant for $k > 500$ m^{-1}—an observation we have found to be true over all the operating conditions where we could resolve the IAT. Given the characteristic axial length scale of the plume in our experiment was ~ 10 cm, the short wavelength of the IAT ($\lambda < 1$ cm) in the axial direction suggests that the results from the kinetic formalism of Sec. II that are valid for a locally uniform plasma may still be applied. We therefore are free to interpret the saturation of the IAT through the lens of kinetic theory, and in the next section, we use this fact to explore how the experimentally-observed amplitude of the IAT compares to our predictions from Sec. II.

C. Power spectra

Now that we have established that ion acoustic turbulence can onset in the cathode plume, we turn our attention to the second question concerning the IAT: what is the character of its frequency spectrum. To this end, we begin by examining the overall amplitude of the IAT and then turn to a discussion of its decay at high frequency.

We show in Fig. 6 for fixed flow rate and increasing discharge current the power spectra of potential oscillations as measured by an on-axis ion saturation probe. It is immediately evident from these plots that the IAT first appears at $I_D \approx 40$A, and although the amplitude of the spectrum decreases at $I_D = 50$ A, it ultimately increases with discharge current. This behavior of the IAT at high currents is consistent with two of our theoretical results from Sec. II.B. First, we saw in this section that the magnitude of the IAT should scale with electron temperature and electron drift. As we can see directly from Fig. 2, the electron temperature does in fact increase with current, and since $I_D \propto n_0 V_e$, we can infer that the electron drift does at least depend weakly on discharge current. Second, the results of Sec. II.B indicate the existence of a maximum in the frequency spectra with $\omega^* \ll \omega_{pi}$. As we can observe from Fig. 6, such a maximum does in fact appear. With respect to the effects of changing flow rate at constant discharge current, we can see from

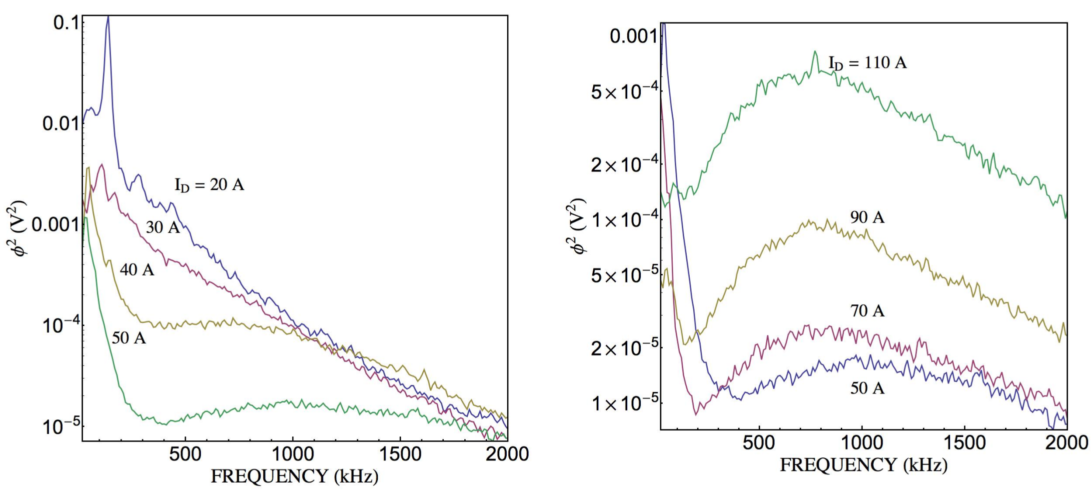

Figure 6. Power spectra for $\dot{m} = 10$ sccm as a function of increasing current. The left hand diagram illustrates the initial emergence of the IAT while the right hand plot shows the growth of IAT with increasing current.

the cases illustrated in Fig. 7 that the amplitude of the power spectrum significantly decreases with flow rate. Based on our expression Eq. 13, this reduction could result from a combination of a number of factors. For example, the decrease in electron temperature with flow rate could lead to a damping of the spectrum, or, as we can see by examining Eq. 13 for frequencies near ω^*, the enhanced ion-neutral collisional damping that results from increased flow rate may reduce the IAT amplitude.

Trends in total amplitude aside, we also need to examine the fall off of the frequency spectrum since this was a key assumption that enabled our estimate for the anomalous collision frequency in Sec. II.C. In particular, we found that if nonlinear wave-wave and wave-particle processes are the dominant process for saturating the IAT, the fall off the spectra should be characterized by a ω^{-3} dependence (Eq. 14). To explore this possibility, we show in Fig. 8 a sample log-log plot of the power spectrum of the IAT where we have fit a line to the drop off in the spectrum that occurs after the peak. The slope of the fitted line is -2.8, which corresponds to a decrease in power spectrum amplitude of $\omega^{-2.8}$. We similarly have examined the

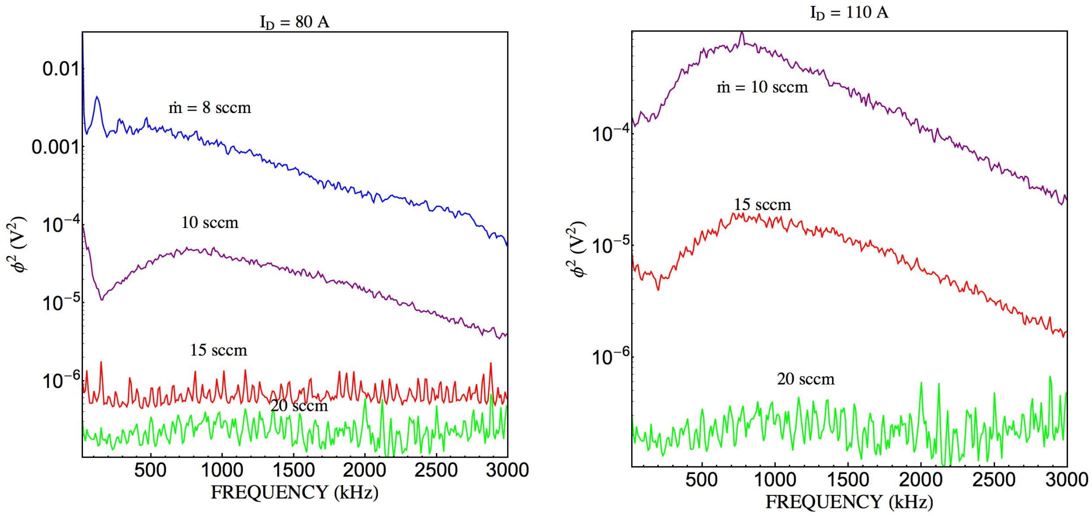

Figure 7. Log plots of power spectra for fixed currents and different flow rates.

decay of the power spectra for all of the flow rate conditions and discharge current values where we could identify from the Beall plot technique that the ion acoustic mode was present. The slopes we found from this parametric investigation are shown on the right side of Fig. 8 along with the theoretical value of the Kadomtsev spectrum.

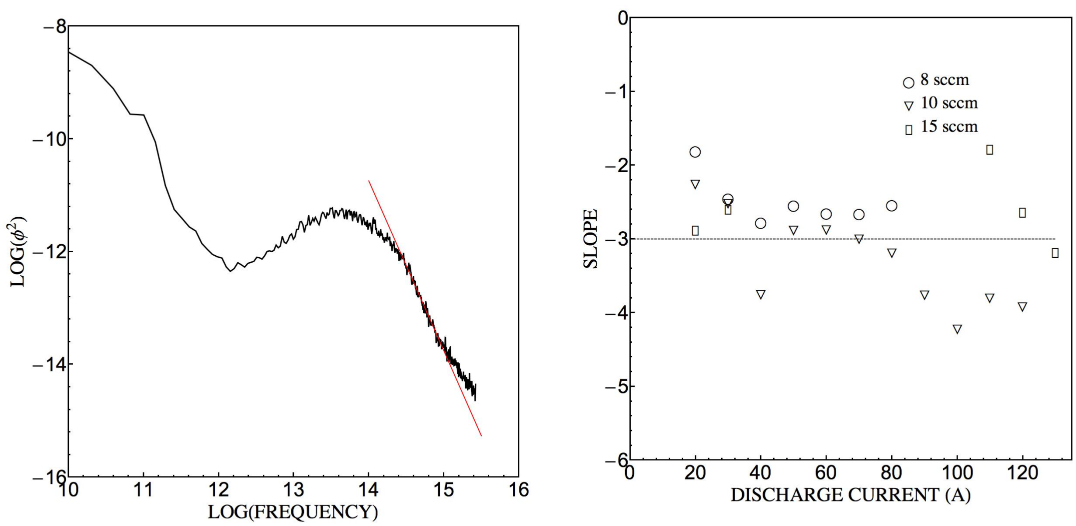

Figure 8. Left: log-log plot of the measured power spectrum at $I_D = 100$A and $\dot{m} = 10$ sccm. The red line is a best fit to the decay of the spectrum. Right: the slopes of the best fits lines as a function of discharge current for three different flow rates. The dotted line indicates the theoretical Kadomtsev value of -3.

The close proximity to theory exhibited over the range of operating conditions in Fig. 8 provides conclusive evidence that the Kadomtsev spectrum and its nonlinear decay is the dominant process for the saturation of the IAT. Armed with this observation, we now can be confident that only does the IAT exist in the cathode plume but we can associate its growth with the anomalous collision frequency given by Eq. 20. In the next section, we evaluate this expression for our experimental measurements of the IAT.

D. Collision frequency

We show in Fig. 9 the anomalous collision frequency of the IAT calculated from our measurements of the power spectrum and Eq. 20. It is apparent from this plot that for the cases where we could detect the IAT, the collision frequency exhibited the same trends as the ones we outlined for the power spectrum amplitude in the previous section: at high discharge currents, the collision frequency increases, and at high flow rates, the collision frequency decreases. This is an unsurprising result given that Eq. 20 depends on the amplitude of the power spectrum. Similarly, since electron resistivity is a function of collision frequency, we can relate

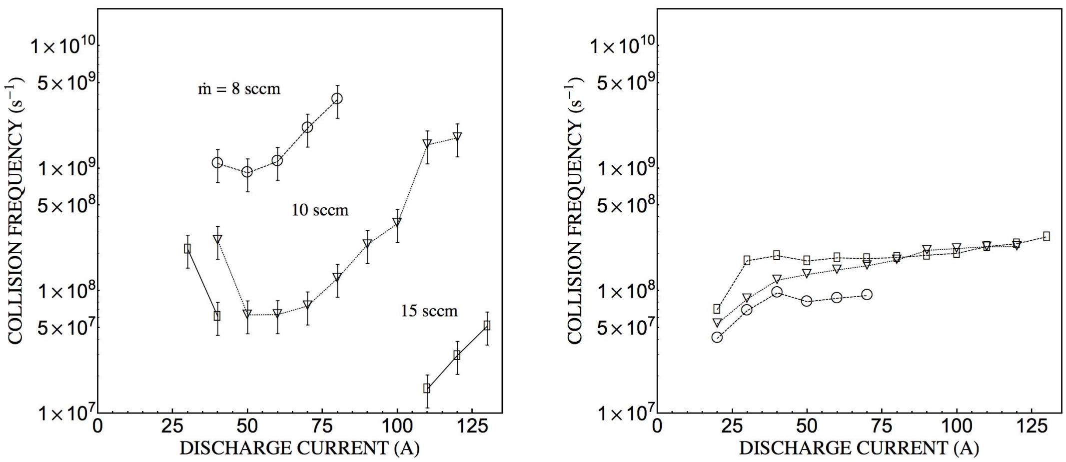

Figure 9. Left: effective collision frequency due to the IAT. Right: the classical electron-ion collision frequency based on measurements of the electron temperature and density. Maximum error is ±30%.

the trends we see in Fig. 9 to the electron temperature results we discussed in Sec. III.A. In particular, we pointed out that the growth of the anomalous collision frequency in the cathode plume may explain the increase in electron temperature with discharge current depicted in Fig. 2. The same trends exhibited by the anomalous collisionality and electron temperature supports this thesis.

In order to evaluate the relative importance of the IAT collision frequency in driving the plasma parameters, we compare our results with the right hand side of Fig. 9. This shows the electron-ion collision frequency based on our measurements of the local electron temperature and density:

$$\nu_{ei} = 2.9 \times 10^{-12} n_0 T_e^{-3/2} \left[23 - 0.5 \log \left(\frac{10^{-6} n_0}{T_e^3} \right) \right], \tag{32}$$

where n_0 is the background density in units of m^{-3}. By comparing the two sides of Fig. 9, we can see that under certain circumstances—a high discharge current to flow rate ratio—the anomalous collision term can be dominant. This is the first experimental evidence that not only are there non-classical effects in the plume, but that these effects can be larger (under the right operating conditions) than classical terms. In turn, this result directly supports the conclusions from previous attempts to model the cathode plasma[1,16,24] where it was found that the steady-state parameters of the cathode plume cannot be explained by ordinary interspecies collisions.

Of course, even though it is evident that the anomalous frequency can exceed the classical term, the question remains as to whether or nor the magnitude of the collision frequency is sufficiently large to explain the enhanced collisionality employed in cathode models. However, in a companion paper[24] simulations of our cathode at the axial position where our measurements were performed have shown that the necessary anomalous collision frequency to accurately capture the measured plasma parameters is $\nu_{AN} \sim 10^8$ s^{-1} for a flow rate of 12 sccm and a discharge current of 100 A. Extrapolating from our results in Fig. 9 suggests that the experimentally measured collision frequency should closely approach this value. The IAT thus is sufficiently large to account for the anomalous resistivity used in this cathode model.

As a final consideration, we recall that since fluid models cannot predict kinetic effects and therefore cannot use Eq. 20 to estimate the anomalous collision frequency, they adopt the Sagdeev form, Eq. 22, for the collision term.[1,16,24] By showing that the IAT spectrum decays in the Kadomtsev sense in Sec. II.C, we have confirmed that this is an appropriate form to model the effects of the IAT. And by demonstrating in this section that the collision frequency we measured matches the modeled collision frequency, we can conclude that Eq. 22 is the only term needed to simulate the anomalous collisionality in the 100-A cathode plume.

E. High energy ion formation

While our investigation has largely been focused on establishing the link between the IAT and anomalous collisions, in this last section, we devote a brief discussion to the role of the IAT as pertains to the second anomalous effect in high-current cathodes: energetic ion production. In particular, we note that while we have found in the previous sections that the IAT grows at the expense of the energy in the electron drift, our experimental measurements of the turbulent spectrum combined with the discussion from Sec. II.B also indicate the major loss mechanisms for the IAT are collisional ion damping and nonlinear ion processes. This suggests that the IAT must deposit at least some energy in the ion population, and indeed, a long history of experiments have causally linked the formation of a high energy ion tail with the onset of IAT in low temperature plasmas.[18–20]

In order to explore the possibility of such a link in our cathode, we have measured the ion energy distribution as a function of discharge current at the flow rate where anomalous collisionality (and therefore the anticipated ion heating) was the largest: 8 sccm. We show the resulting normalized RPA traces as well as the inferred ion energy distributions (assuming dominant single charge states) as functions of increasing current in Fig. 10. As we can see, each energy distribution plot exhibits a peak in the $15 - 20$ V range. This is a characteristic value on the order of the discharge voltage that reflects the energy gained by ions as they fall through the steady-state potential of the plasma.[15] With increasing discharge current, however, we note a tail begins to form in the higher energy range $50 - 80$ V. This development is consistent with previous investigations of unmagnetized hollow cathode plumes where it was noted that since the energy in the tail greatly exceeds the most probable value, there must be an anomalous acceleration mechanism that develops at high current discharge currents.[9]

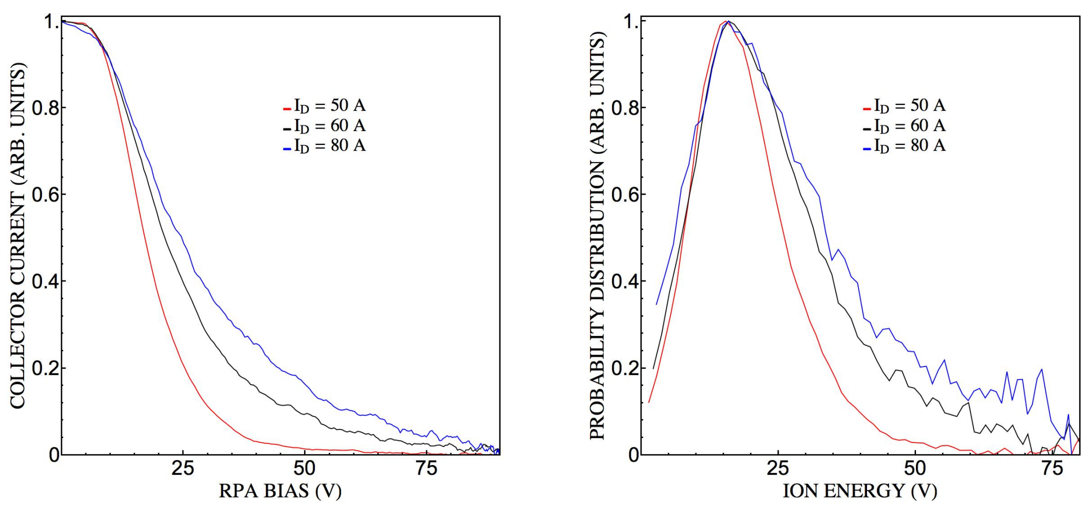

Figure 10. Left: ion collector current as a function of RPA bias voltage for $\dot{m} = 8$ sccm. Right: the probability distribution of the ion energy subject to the assumption of singly charged ions. Three cases for discharge current are shown, and all traces have been normalized to their maximum value.

Our observation of the IAT's increasing amplitude with discharge current along with the growth of the ion tail with the same operating parameter suggests that the IAT may be this anomalous acceleration mechanism. However, while the relationship between IAT growth and energetic ions has been demonstrated to be causal in other experimental investigations;[19] we stress here that we have not established such a link in our experiment. This would require a more in-depth examination of the mechanisms by which the IAT can transfer energy to the ion tail, which is beyond the scope of this paper. Thus, while we have found that the IAT is directly responsible for the first anomalous effect—enhanced collisionality—we only can conclude here that the link between the IAT amplitude and the formation of energetic ions is correlational.

V. Discussion

We can summarize the results from our theoretical and experimental work concerning the contribution of the IAT to the anomalous collision frequency with the following observations:

1. The IAT exists in the hollow cathode plume.
2. The IAT spectrum has a Kadomtsev-like decay at high frequencies.
3. The experimentally measured anomalous collision frequency exceeds classical frequencies for high current densities.
4. The measured anomalous collision frequency closely matches the value required to successfully capture the plasma parameters in a simulation of the 100-A cathode.

These observations have a direct impact on our understanding of the underlying physical processes in the hollow cathode plume. In particular, for sufficiently high current to flow ratios, the anomalous collision frequency from the IAT cannot be ignored. Rather, this effect must be taken into consideration if we want to successfully model the plasma parameters such as potential, electron temperature, and density in the cathode plume. Creating models capable of such high fidelity is essential both for efforts to model long-term cathode behavior as well as attempts to realize new designs. These capabilities will become increasingly important as the next generation of missions calls for cathodes with higher discharge currents.

In terms of the second anomalous process in high current cathodes—energetic ion production— we have shown theoretically how there is a process for IAT to transfer energy to the ions: the waves are driven unstable at the expense of energy in the electron drift while the waves in turn transfer energy to the ions through collisional and nonlinear processes. Our experimental work similarly has demonstrated a correlation between the formation of a high energy ion tail and the onset of IAT. In light of these results, we believe that exploring a causal link between these two processes may be critical toward future efforts to improve cathode lifetime. This work represents a first step toward this end.

VI. Conclusion

In this work, we have presented a parametric investigation of ion acoustic turbulence in the plume of a 100-A LaB_6 cathode. We have reviewed the theory for how IAT can lead to the onset of anomalous collisions at the expense of the current in the hollow cathode discharge, and we have shown how we can calculate the collision frequency associated with the IAT provided the IAT spectrum has a certain shape. Through a series of probe-based investigations, we have implemented an experimental setup in which we were able to detect successfully the onset and growth of the IAT at high discharge current. We furthermore have investigated the details of the power spectra exhibited by these waves over a wide range of discharge current and flow rate. Our findings match the predictions of turbulent kinetic theory, and this correspondence suggests the following mechanism for IAT onset: while the IAT is driven unstable by electron drift, nonlinear processes lead to a redistribution of the wave energy from high frequencies to low values while ion collisional damping leads to cutoff of the wave at low frequencies.

Through direct measurement, we have confirmed that the anomalous collisionality from the IAT is dominant over classical processes at high discharge currents, and we have demonstrated how the agreement between the kinetic theory and our experimental measurements lends support to the use of anomalous collisionality in models of the hollow cathode. In particular, the collision frequency we measured for a high current case closely matched the value employed in a companion paper that successfully modeled the plasma parameters in our 100-A LaB_6 cathode.[24] We also have shown that there is a correlation between an increase in the energy in the IAT and the formation of a high energy ion tail. While we did not establish a causal relationship between these two mechanisms, the historical precedent for the production of high energy ions in the presence of IAT suggests that our observed link between the two processes should be further explored.

In sum, we believe this work will help enable future missions in two ways. First, by identifying the IAT as a main contributor to the collisionality in the hollow cathode plume and by confirming the validity of a first-principles expression for the magnitude of the resulting collision frequency, we believe our results will help improve future models for hollow cathode performance. And second, in light of the correlation between the IAT's growth and ion energy, we believe our conclusions concerning the factors governing the steady-state IAT may contribute to an improved understanding of the mechanisms behind the formation of energetic ions. Both of these insights will become increasingly important as the need for higher current cathodes becomes more pressing.

Acknowledgments

The research described in this paper was carried out by the Jet Propulsion Laboratory, California Institute of Technology, under a contract with the National Aeronautics and Space Administration and funded through the internal Research and Technology Development program.

References

[1]Mikellides, I. G., Katz, I., Goebel, D. M., and Jameson, K. K., "Evidence of nonclassical plasma transport in hollow cathodes for electric propulsion," *Journal of Applied Physics*, Vol. 101, No. 6, 2007, pp. 063301.

[2]Polk, J., Anderson, J., Brophy, J., Rawlin, V., Patterson, M., Sovey, J., and Hamley, J., "An overview of the results from an 8200 hour wear test of the NSTAR ion thruster," *AIAA Paper, 99-2446. June, 1999*.

[3]Sengupta, A., Brophy, J. R., and Goodfellow, K. D., "Status of the extended life test of the Deep Space 1 flight spare ion engine after 30,352 hours of operatio," *AIAA Paper, 03-4558. July, 2003*.

[4]Rayman, M. D., "The Successful Conclusion of the Deep Space 1 Mission: Important Results without a Flashy Title," *IAF abstracts, 34th COSPAR Scientific Assembly*, Jan. 2002.

[5]Koppel, C., Marchandise, F., Prioul, M., Estublier, D., and Darnon, F., "The SMART-1 Electric Propulsion Subsystem around the Moon: In Flight Experience," *41st Joint Propulsion Conference and Exhibit, Tucson,AZ, 10-13 July 2005. AIAA 2005-3671.*, 2005.

[6]Garner, C., Brophy, J., Mikes, S., and Rayman, M., "In-Flight Operation of the Dawn Ion Propulsion System- The First Nine Months," *44th AIAA/ASME/SAE/ASEE Joint Propulsion Conference, 20-23 July, 2008, Hartford, CT. AIAA-2008-4917*, 2008.

[7]Brophy, J. R., Polk, J. E., Randolph, T. M., and Dankanich, J. W., "Lifetime Qualification of Electric Thrusters for Deep-Space Missions," *44th Joint Propulsion Conference, AIAA-2008-5184, Hartford, CT*, 2008.

[8]Brophy, J. and Garner, C., "Tests of High-Current Cathodes for Ion Engines," *AIAA/ASME/SAE/ASEE 24th Joint Propulsion Conference,Boston, MA*, No. AIAA Paper 88-2193, 1988.

[9]Friedly, V. and Wilbur, P., "High current hollow cathode phenomena," *Journal of Propulsion and Power*, Vol. 8, No. 3, 2008, pp. 635–643.

[10]Kameyama, I., "Effects of Neutral Density on Energetic Ions Produced Near High-Current Hollow Cathodes,," Tech. Rep. NASA CR-204154, Oct. 1997.

[11]Williams, G., Domonkos, M. T., and Chavez, J. M., "Measurement of doubly charged ions in ion thruster plumes," *27th International Electric Propulsion Conference, Pasadena, CA, IEPC-01-310*, 2001, pp. 15–19.

[12]Katz, I., Mikellides, I. G., Goebel, D. M., Jameson, K. K., and Johnson, L., "Production of high energy ions near an ion thruster discharge hollow cathode," *42nd AIAA/ASME/SAE/ASEE Joint Propulsion Conference and Exhibit, Sacramento, CA, 2006. AIAA-2006-4485*, 2006.

[13]Foster, J. E. and Patterson, M. J., "Downstream Ion Energy Distributions in a Hollow Cathode Ring Cusp Discharge," *Journal of Propulsion and Power*, Vol. 21, No. 1, Jan. 2005, pp. 144–151.

[14]Gallimore, A. and Rovey, J., "Erosion Processes of the Discharge Cathode Assembly of Ring-Cusp Gridded Ion Thrusters," *Journal of Propulsion and Power*, Vol. 23, No. 6, 2007, pp. 1271–1278.

[15]Goebel, D. M., Jameson, K. K., Katz, I., and Mikellides, I. G., "Potential fluctuations and energetic ion production in hollow cathode discharges," *Physics of Plasmas*, Vol. 14, No. 10, 2007.

[16]Mikellides, I. G., Katz, I., Goebel, D. M., Jameson, K. K., and Polk, J. E., "Wear Mechanisms in Electron Sources for Ion Propulsion, II: Discharge Hollow Cathode," *Journal of Propulsion and Power*, Vol. 24, No. 4, July 2008, pp. 866–879.

[17]Chu, E., Goebel, D. M., and Wirz, R. E., "Reduction of Energetic Ion Production in Hollow Cathodes by External Gas Injection," *Journal of Propulsion and Power*, Vol. 29, No. 5, June 2013, pp. 1155–1163.

[18]Bychenkov, V., Silin, V., and Uryupin, S., "Ion-acoustic turbulence and anomalous transport," *Physics Reports*, Vol. 164, No. 3, 1988, pp. 119 – 215.

[19]de Kluiver, H., Perepelkin, N., and Hirose, A., "Experimental results on current-driven turbulence in plasmas - a survey," *Physics Reports*, Vol. 199, No. 6, 1991, pp. 281 – 381.

[20]Horton, W., *Turbulent Transport in Magnetized Plasmas*, World Scientific, 2012.

[21]Sagdeev, R. and Galeev, A., *Nonlinear plasma theory*, Frontiers in physics, W. A. Benjamin, 1969.

[22]Fitzgerald, D., *Plasma Fluctuations in Ion Thrusters Utilizing Hollow Cathodes*, Ph.D Thesis, Colorado State University, 1983.

[23]Farnell, C., *Plasma Flow Field Measurements Downstream of a Hollow Cathode*, Ph.D Thesis, Colorado State University, 2007.

[24]Mikellides, I. G., Goebel, D. M., Jorns, B. A., Polk, J., and Guerrero, P., "Numerical Simulation of the Partially-ionized Gas in a 100-A LaB6 Hollow Cathode," *33rd International Electric Propulsion Conference, The George Washington University, Washington, D.C. October 6 10, 2013. IEPC-2007-124*, 2013.

[25]Fenneman, D. B., Raether, M., and Yamada, M., "Ion-acoustic instability in the positive column of a helium discharge," *Physics of Fluids*, Vol. 16, No. 6, 1973, pp. 871–878.

[26]Stix, T., *Waves in Plasmas*, AIP, New York, 1992.

[27]Stringer, T., "Low-frequency waves in an unbounded plasma," *Journal of Nuclear Energy. Part C, Plasma Physics, Accelerators, Thermonuclear Research*, Vol. 5, No. 2, 1963, pp. 89.

[28]Kadomtsev, B., *Plasma turbulence*, Academic Press, 1965.

[29]Choi, D.-I. and Wendell Horton, J., "Modified Kadomtsev spectrum from renormalized plasma turbulence theory," *Physics of Fluids*, Vol. 17, No. 11, 1974, pp. 2048–2060.

[30]Tsytovich, V. and Terhaar, D., *Lectures on Non-Linear Plasma Kinetics*, Springer Series on Atomic, Optical, and Plasma Physics, Springer London, Limited, 2011.

[31]Chu, E. and Goebel, D. M., "High-Current Lanthanum Hexaboride Hollow Cathode for 10-to-50-kW Hall Thrusters," *Plasma Science, IEEE Transactions on*, Vol. 40, No. 9, 2012, pp. 2133–2144.

[32]Chen, F. F., "Langmuir probe diagnostics," *Mini-Course on Plasma Diagnostics, IEEE-ICOPS Meeting, Jeju, Korea*, 2003.

[33]Hutchinson, I., *Principles of Plasma Diagnostics*, Cambridge University Press, 2005.

[34]Beall, J. M., Kim, Y. C., and Powers, E. J., "Estimation of wavenumber and frequency spectra using fixed probe pairs," *Journal of Applied Physics*, Vol. 53, No. 6, 1982, pp. 3933–3940.

[35]Williams, G.J., J., Smith, T., Domonkos, M., Gallimore, A., and Drake, R., "Laser-induced fluorescence characterization of ions emitted from hollow cathodes," *Plasma Science, IEEE Transactions on*, Vol. 28, No. 5, 2000, pp. 1664–1675.